Uptake of Ra during the recrystallization of barite: a microscopic and ToF-SIMS study

Martina Klinkenberg[1,*], *Felix Brandt*[1], *Uwe Breuer*[2], *Dirk Bosbach*[1]

[1]Institute of Energy and Climate Research (IEK-6) – Nuclear Waste Management and Reactor Safety, Research Centre Jülich GmbH, 52425 Jülich, Germany

[2]Central Institute of Engineering, Electronics and Analytics, ZEA-3 Analytics, Research Centre Jülich GmbH, 52425 Jülich, Germany

Keywords: Barite, Radium, solid solution, recrystallization, ToF-SIMS, nuclear waste repository

A combined macroscopic and micro analytical approach was applied on two distinct barite samples from Ra uptake batch experiments using ToF-SIMS and detailed SEM investigations. The experiments were set up at near to equilibrium conditions in order to distinguish between two possible scenarios for the uptake of Ra by already existent barite, (1) formation of a $Ba_{1-x}Ra_xSO_4$ solid solution surface layer on the barite or (2) a complete recrystallization, leading to homogenous $Ba_{1-x}Ra_xSO_4$ crystals. It could be clearly shown that Ra uptake in all barite particles analyzed within this study is not limited to the surface but extends to the entire solid.

For most grains a homogenous distribution of Ra could be determined, indicating a complete recrystallization of barite into a $Ba_{1-x}Ra_xSO_4$ solid solution. The maxima of the Ra/Ba intensity ratio distribution histograms calculated from ToF-SIMS are identical with the expected Ra/Ba ratios calculated from mass balance assuming a complete recrystallization.

In addition, the role of Ra during the recrystallization of barite was examined via detailed SEM investigations. Depending on the type of barite used, an additional coarsening effect or a strong formation of oriented aggregates was observed compared to blank samples without Ra. In conclusion, the addition of Ra to a barite at close to equilibrium conditions has a major impact on the system leading to a fast re-equilibration of the solid to a $Ba_{1-x}Ra_xSO_4$ solid solution and visible effects on the particle size distribution, even at room temperature.

Introduction

The system $RaSO_4 – BaSO_4 – H_2O$ is a classic example of solid solution formation. Already in 1925, the publication by Doerner & Hoskins (1) postulated a structural uptake of Ra into the crystal structure of barite during co-precipitation of Ra and Ba with sulfate. Especially the isotope ^{226}Ra which yields a series of short lived decay products is known to be a major environmental concern which easily enters the food chains (2).

Due to the environmental relevance as one of the major sources of technologically enhanced naturally occurring radioactive material (TENORM), the fate of Ra in the environment and in technical processes has been the subject of several publications (e.g. 3, 4, 5, 6, 7). On the short time scale of hours to days which is relevant for processes such as unconventional gas extraction the mechanism of co-precipitation of Ra from supersaturated solutions dominates the

sequestration of Ra from aqueous solutions whereas the uptake of Ra by pre-existing barite is too slow to be relevant (8).

However, the uptake of Ra by pre-existing barite at close-to equilibrium conditions is relevant for the safety assessment of nuclear waste disposal which are carried out to cover the complete time span until natural levels of radiation are reached. Barium is formed from the decay of Cs and as a fission product (^{138}Ba). ^{138}Ba already exists within the fuel elements during the production of nuclear power. On the other hand, Ra as a late decay product of the ^{238}U is formed after 10,000 to 100,000 years. Especially in the late stages of direct disposal of spent nuclear fuel (300.000 years), Ra may become the dominant source of radioactivity (9, 10). Here, a particular scenario may be considered: During spent fuel corrosion Ba is released from the waste matrix as a fission product and at the same time UO_2 dissolves. ^{226}Ra forms as a daughter nuclide within the decay chain of ^{238}U, which may be released from the UO_2. Based on thermodynamics, eventually the released Ra should re-equilibrate with the earlier formed barite and form a $Ba_{1-x}Ra_xSO_4$ solid solution.

Several recent theoretical studies have focused on the estimation of Ra mobility in ground waters which may come into contact with spent fuel in a radioactive waste repository (10, 11, 12, 13). The possible solubility control of Ra by coprecipitation of a $Ba_{1-x}Ra_xSO_4$ solid solution from high supersaturation has been demonstrated in recent publications (14, 15, 16). Recently, experimental and modeling approaches were used to derive the thermodynamic constants needed to describe the solid solution and the speciation of the aqueous solution in equilibrium (14, 15, 16, 17).

However, the scenario which may be applied to the direct disposal of spent fuel in a deep geological waste repository requires the uptake of Ra by barite at close to equilibrium conditions.

This scenario has been addressed by recent macroscopic experimental studies of Curti et al., 2010 (18) and Bosbach et al., 2010 (19). The available macroscopic results indicate a partial or full recrystallization of barite to $Ba_{1-x}Ra_xSO_4$ solid solution combined with a significant reduction of the Ra in aqueous solution. In these studies, it is argued that the initial pure barite either recrystallized completely (18) or incompletely (19) to a $Ba_{1-x}Ra_xSO_4$ solid solution. In the latter case, kinetic inhibition was invoked as an explanation. However, in their discussion of the data of Bosbach et al., 2010 (19), Vinograd et al., 2013 (17) point to a full recrystallization of barite to a $Ba_{1-x}Ra_xSO_4$ solid solution within the scale of the experiments. Therefore, based on the available macroscopic data it remains unclear whether a $Ba_{1-x}Ra_xSO_4$ solid solution is only formed as a surface layer on the barite crystals or if a complete recrystallization occurs, leading to homogenous $Ba_{1-x}Ra_xSO_4$ crystals.

Here we present new experimental results, following a combined macroscopic and microanalytical approach. Batch experiments with higher Ra concentrations than published so far were carried out in order to analyze the spatial distribution of Ra within the solid after the recrystallization experiments as well as the effect of the presence of Ra on the morphology and particle size distribution (PSD).

Materials and Methods

Barite sample preparation and characterization

Two different types of barite powders with varying grain size distribution and morphology were used during the Ra uptake experiments. The first barite was a synthetic, high purity barite (XR-HR10) from Sachtleben Chemie® GmbH, which was provided by Enzo Curti (Paul Scherrer Institute, Villigen, Switzerland). The same barite was used in the experiments of Curti

et al., 2010 (18) and Bosbach et al., 2010 (19). The second barite was a commercially available barium sulfate from Aldrich with a purity of 99.998 %. Several equilibration steps were carried out to eliminate high energy surface sites and ultrafine particles which may have a high impact on the Ra uptake kinetics. In a first step, the barite powders were equilibrated in pure water for 6 weeks. Afterwards, a grain size fractionation was carried out via sedimentation using Atterberg cylinders to narrow down the grain size distribution of the two barite types and achieve a homogeneous PSD. Thus, two distinctively different barite powder samples were prepared, a coarse Sachtleben (SL) barite with a mean particle size of approximately 18 µm and a fine grained Aldrich (AL) barite with a mean particle size of approximately 0.5 µm.

The original barite samples were analyzed by powder X-ray diffraction using a Bruker D4 Endeavor instrument. The morphology of the barite crystals before and after the adjustment of the grain size distribution was studied using the environmental scanning electron microscope FEI Quanta 200 F. The microscope was equipped with an Apollo X Silicon Drift Detector (SDD) from EDAX.

XRD and SEM/EDX confirmed that both powders were pure barite within the precision of these methods. SEM observation showed that SL barite consisted of blocky crystals with a wide grain size distribution, whereas the original AL sample consisted of two different barite morphologies.

SEM observation after separation and equilibration indicated that the AL barite consisted of rounded particles forming agglomerates. The particles showed smooth crystal surfaces with small pores. The mean particle size was < 2 µm. The separated SL barite consisted of blocky crystals with a particle size of > 10 µm. The SL morphology was dominated by barite cleavage planes.

The specific surface area of the separated powder samples was determined via multipoint Kr-BET measurements. A Quantachrome Autosorb instrument was used to obtain 5-point isotherms of about 0.5 g of each sample. Previously, the samples were outgassed at 120 °C for 14 h. The specific surface area of Sachtleben barite was S_{BET} = 0.17 m²/g, and differed from the specific surface area of S_{BET} = 0.31 m²/g determined by Curti et al., 2010 (18). This may be due elimination of fine particles following the size fractionation procedure. The specific surface area of the Aldrich barite was determined as S_{BET} = 1.7 m²/g.

Ra uptake experiments

Batch recrystallization experiments were performed at ambient conditions (23 ± 2 °C). The separated and pre-equilibrated barite powders were suspended in 10 mL of 0.2 n NaCl solutions for 4 weeks in 25 mL glass bottles. A stock solution with a concentration of $8.8 \cdot 10^{-4}$ mol/L ^{226}Ra was prepared from $RaBr_2$ and diluted to 1.0 x 10^{-5} mol/L.

At the beginning of the ^{226}Ra uptake experiments, 10 mL of the radiotracer solution were added to each of the barite suspensions, resulting in a total volume of V = 20 mL, an ionic strength of 0.1 n, and a concentration of 5.0 x 10^{-6} mol/L ^{226}Ra. The ionic strength was chosen to address the conditions expected for the Swedish granitic groundwater (20). Experiments were carried out with two different solid/liquid ratios of 5 g/L and 0.5 g/L (Table 1). The glass bottles with suspensions were permanently shaken with a roller mixer shaker. Furthermore, two types of blank experiments were conducted - (1) blank experiment without barite to evaluate the adsorption of Ra on the glass bottles and (2) a blank experiment with barite but without Ra in order to compare the morphological evolution of the barite crystals in the presence and absence of Ra (Table 1).

In regular time intervals, 500 µL of the aqueous solution were taken and then filtered after a settling time of 1 h. Similar to the procedure described in Curti et al., 2010 (18), the liquid was filtered through Advantec ultrafilters (MWCO = 10,000 Da) and then analyzed for the Ra and Ba concentration.The Ra concentration in solution was examined via Gamma spectrometry. For this purpose, 100 µL of the filtered solution were measured using a N_2 cooled high purity (HP) Ge-detector. Gamma-W for Windows was used for the analysis of the spectra (Version 2.55, Interaktive Spektrum Analyse, Dr. Westmeier, Gesellschaft für Kernspektrometrie mbH). The intensity in counts per second of the Ra peak at 186 keV was determined and converted to a concentration in mol/L. The system was calibrated with an independent, external standard.

The Ba concentration in solution was quantified via ICP-MS. Measurements were performed with an ICP-MS ELAN 6100 DRC (PerkinElmer SCIEX) instrument. For the measurements, the samples were diluted by a factor of 1:100 and acidified (HNO_3).

Analysis of the solids

Scanning electron microscopy (SEM):

Small amounts of barite (10 µL suspension) were sampled during the recrystallization experiments. The evolution of the barite crystals morphology was studied using the environmental scanning electron microscope FEI Quanta 200 FEG. In order to avoid artifacts due to precipitation of NaCl, $BaSO_4$ or $RaSO_4$, the samples were separated from their solution by two washing steps in iso-propanol. The samples were then prepared as a suspension on a Si wafer and subsequently dried.

Determination of the particle size distribution by image analysis:

For the AL samples, the longest axis of 360 grains of each sample was measured via image analysis of SEM images at 40,000 x and 20,000 x magnifications. Due to the larger grain size of the SL barite and narrow grain size distribution, 150 grains per SL sample were analyzed for images taken at a magnification of 1800 x and 2000 x. A control sample of 350 grains showed that analyzing 150 grains was sufficient to obtain reproducible results of this sample. Grains, which were grown together, were considered individually and not as a single grain. For each sample, the minimum and maximum grain sizes as well as the mean values of the analyzed grains were determined. The equivalent mass of each grain was calculated using the measured grain size as the diameter of an equivalent sphere and the density of barite (4.5 g/cm³).

Time of flight secondary ion mass spectrometry (ToF-SIMS)

Time of flight secondary ion mass spectrometry (ToF-SIMS) has found wide application within the last decades in the ultra-trace element analysis of solids with a high spatial and mass resolution (21). Within this study, a method was developed specifically for the analysis of the recrystallized barite grains and the detection of Ra in the sub-ppm range.

Small amounts of powder samples were taken for ToF-SIMS measurements after characterization by SEM and prepared for ToF-SIMS. SIMS measurements were carried out using a ToF-SIMS IV instrument (IONTOF GmbH, Münster Germany). For the mass spectral analysis a pulsed Bi^{3+} beam of 25 keV was used. The beam was raster scanned over a max area of 500 x 500 µm. To gain access to the depth distribution of elements and isotopes a sputter beam of 2 keV Cs^{+} was scanned over the area of interest. The sputtered ions were accelerated by 2 keV extraction voltage into the reflectron type drift tube. The high flexibility of ToF-SIMS in

176 selecting the sputter and analysis timing independently (22) allowed us to address the different
177 particle sizes.

178 During the ToF-SIMS measurements, a special focus was laid on the spatial resolution so that
179 individual barite grains could be distinguished from one another in the SL sample. In addition,
180 the sputter time and sputter conditions were set so that a relevant Ra signal could be extracted
181 from the measurements with a depth resolution of about 0.1 µm within the depth profiles, and a
182 lateral resolution of about 2 µm as estimated from a comparison of SEM and ToF-SIMS
183 analyses. The small particles were sputtered with relative low sputter ion density to use as much
184 material for the acquisition to gain enough sensitivity. To identify individual particles the spot
185 size of the analysis beam had to be improved. This was done by not using the buncher to gain
186 high mass resolution. This reduces the energy spread in the Bi pulse and therefore yields a better
187 focus. The high mass resolution was not necessary and this was verified by looking at the mass
188 spectra for Ra containing and Ra free barite samples. Different masses were tested e.g. the mass
189 of ^{226}Ra, ^{226}RaH, and ^{226}RaO before the mass of 226 was chosen. At this mass, the AL and SL
190 blank samples clearly showed no Ra signal whereas Ra could be detected within the
191 recrystallized samples.

192 Figure 1 shows SEM images of a SL-type barite before and after a ToF-SIMS measurement.
193 The element contrast of the back scattered electron-image (BSE) in Figure 1 b shows a complete
194 sputtering of the sample with very small residues of the original barite left on the substrate. The
195 elevated features of Figure 1 b are due to the protection of the silicon substrate by the barite
196 particles during sputtering.

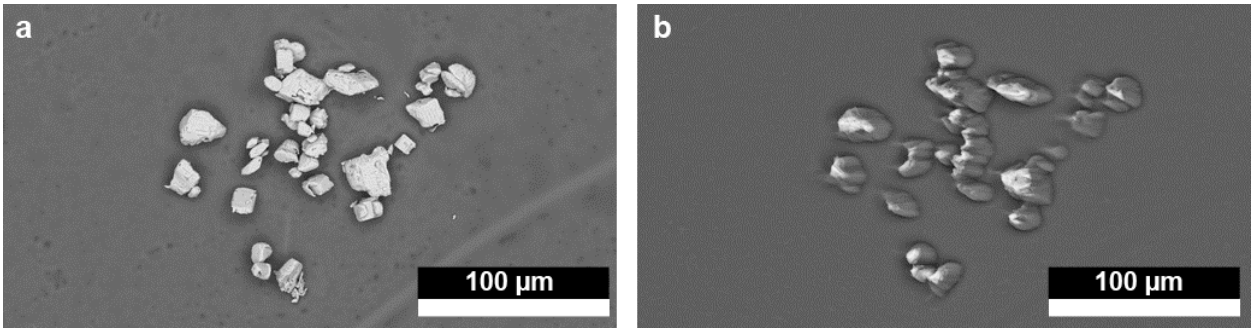

Figure 1. SEM images of ToF-SIMS preparation of SL 0.5 g/L before (a) and after measurement with residues of barite on the Si-substrate at the original location of the barite particles (b).

The measurement raw data were processed with the IONTOF software surfaceLab6 Version 6.3 and reconstructed to obtain three dimensional element distribution images. From the element distribution images, element profiles were calculated as well as the integrated intensity of the Ba or Ra signal at a defined x-y position.

Results and Discussion

Uptake of Ra during barite recrystallization

Final Ra concentration in aqueous solution

The Ra concentration in solution significantly decreased during 443 days of experiment. The final concentrations are given in Table 1. The experiments with 5 g/L barite the Ra concentration showed a decrease from 5.0×10^{-6} to the order of 10^{-9} mol/L whereas the Ra concentration in solution of the 0.5 g/L experiments decreased to the order of 10^{-8} mol/L. According to these results, a Ra/Ba ratio of the solid was calculated from mass balance. In both cases, almost all of the Ra in solution is taken up into the given amount of barite, leading to a Ra/Ba = 2.5×10^{-4} for the experiments with S/L = 5 g/L barite whereas for S/L = 0.5 g/L barite the Ra/Ba ratio was calculated to be one order of magnitude higher (Table 1).

Table 1. Overview of experiments and final Ra concentration after 443 days.

Name	Type of barite	Solid/Liquid	Initial Ra concentration	Final Ra concentration	Ra/Ba in the solid
		[g/L]	[10^{-6} mol/L]	[10^{-9} mol/L]	[-]
Blank Ra	---	---	5	5000 ± 200	
Reference SL	Sachtleben	5	0		
Reference AL	Aldrich	5	0		
SL 0.5 g/L	Sachtleben	0.5	5	35 ± 10	2.5×10^{-3}
SL 5 g/L	Sachtleben	5	5	2.8 ± 0.8	2.5×10^{-4}
AL 0.5 g/L	Aldrich	0.5	5	47 ± 14	2.5×10^{-3}
AL 5 g/L	Aldrich	5	5	7.4 ± 2.2	2.5×10^{-4}

ToF-SIMS investigations of the final Ra concentration and distribution in the solid phase

Due to the larger grain size, the SL sample was chosen for a detailed ToF-SIMS investigation of the spatial distribution of Ra and the total Ra/Ba ratio. Individual grains could be identified by comparing a SEM image taken before the measurement (Figure 2 a) with the integrated intensity distribution image of Ba (Figure 2 b) and Ra (Figure 2 c). Additional measurements were carried out on AL-type barite, on which due the smaller particle size only integrated Ra/Ba ratios over several grains could be determined.

A comparison of the images showing the integrated Ba and Ra ToF-SIMS signal (Figure 2 b,c) and the SEM image (Figure 2 a) shows a good correlation between the areas of high integrated intensities in the ToF-SIMS images and the spatial distribution of the grains in the SEM image. Furthermore, it can be seen in Figure 2 that all grains within this measurement of the recrystallized SL barite contain Ra. Additional ToF-SIMS measurements on different grains of the same sample which are not shown here, confirmed that this is typical for the recrystallized SL barite.

For the four grains identified in the ToF-SIMS image (labeled 1 to 4 in Figure 1 a) depth profiles were reconstructed using the IONTOF software (Figure 2 d). The four grains had similar dimensions (Figure 2 a) and were sputtered completely. Even though the absolute height scale is not measured by ToF-SIMS, the profiles represent the same length as they were taken during the same measurement. For the same reason the total concentrations depicted in the profiles are directly comparable. The profiles indicate a complete recrystallization of barite to a $Ba_{1-x}Ra_xSO_4$ solid solution on the scale of the ToF-SIMS instrument. All SL grains which were analyzed indicate measurable concentrations of Ra not only on the surface but also within the grains. Grain 1 and 4 in Figure 2 d show a slight inhomogeneity of the Ra concentration whereas grain 2 and 3 are homogeneous with regard to the Ra concentration. The total Ra concentration within the grains varies as can be seen by the total counts (TC) depicted in Figure 2.

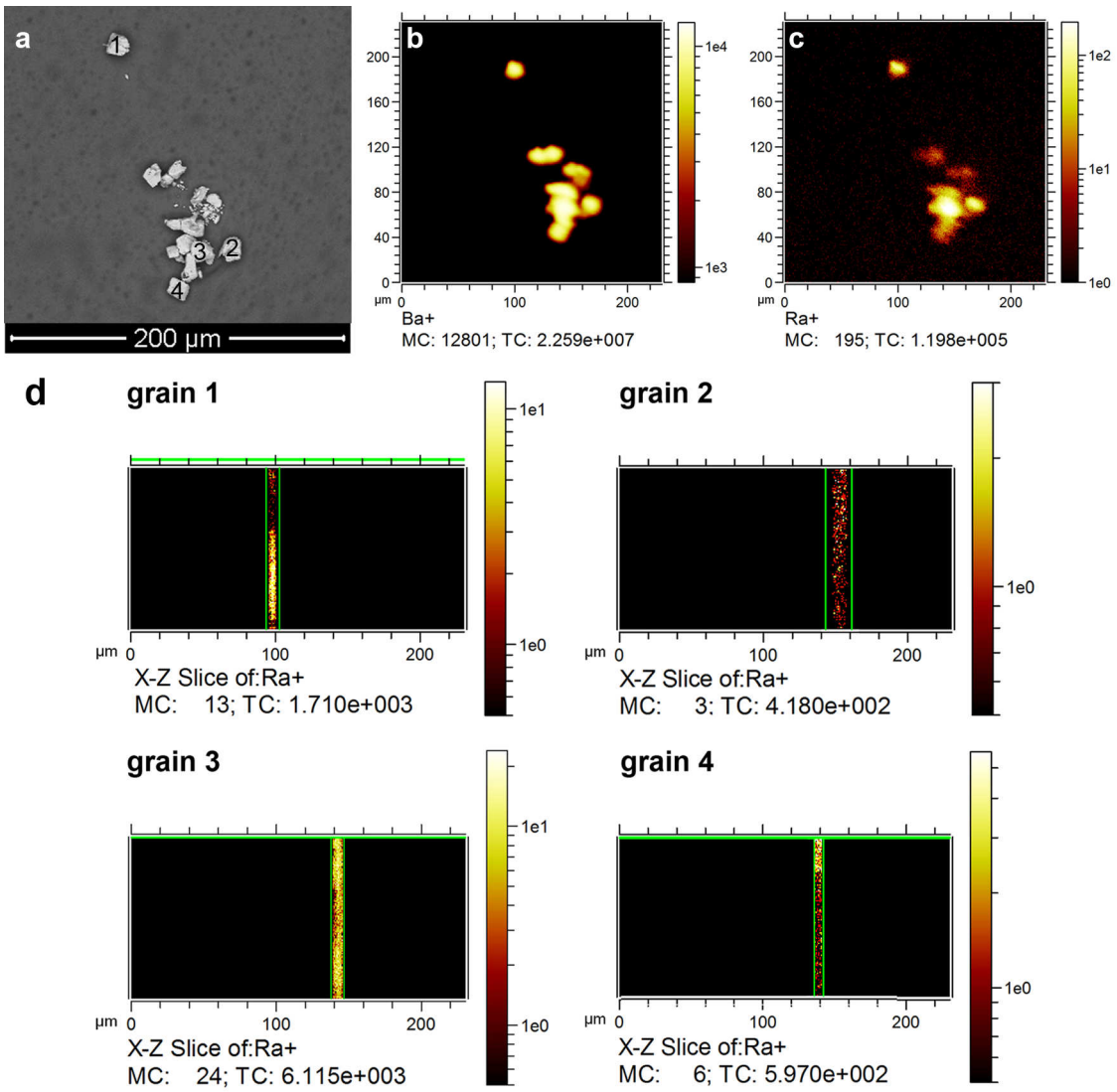

Figure 2. a) SEM image of SL 0.5 g/L before the ToF-SIMS analysis, b) integrated intensity of the Ba signal c) integrated intensity of the Ra signal. MC = Maximum Counts, TC = Total counts. d) Depth profiles of the integrated Ra signal. The x-axis of the depth profiles corresponds with the x-axis of the integrated intensity distribution image (c). The y-axis of the depth profiles are given in arbitrary units as the ToF-SIMS does not provide an absolute height scale.

Absolute concentrations of Ra and Ba in the ToF-SIMS measurements are difficult to determine due to the absence of suitable Ra standards. However, assuming a similar yield of

252 secondary ions of Ba and Ra, a Ra/Ba ratio of the recrystallized barite can be determined from
253 ToF-SIMS measurements. The intensities of Ra and Ba are related to the number of atoms which
254 are ionized and can thus be used to estimate the molar ratio of Ra/Ba. As shown in Table 1, the
255 average Ra/Ba ratio of 2.5 x 10^{-3} is expected in both SL and AL grains. The Ra/Ba ratios
256 determined from several hundred integrated Ra and Ba intensities show a distribution of Ra/Ba
257 intensity ratios rather than one single Ra/Ba ratio in both recrystallized barite samples (Figure 3).
258 Both intensity distributions have a maximum at a Ra/Ba ratio of about 3 x 10^{-3}.

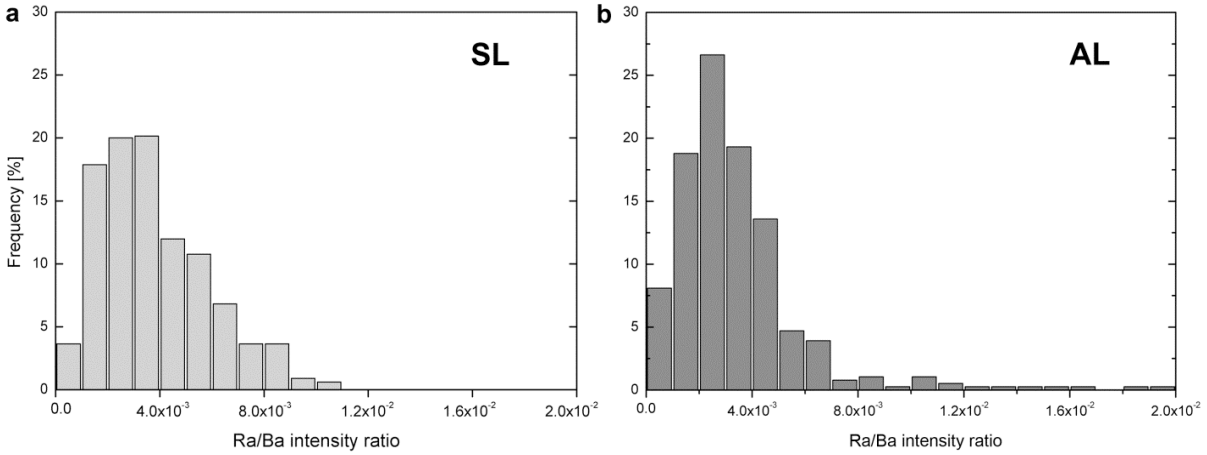

259

260 **Figure 3.** (a) Histogram of the Ra/Ba ToF-SIMS intensity ratio obtained from 660 integrated
261 measurement points of SL 0.5 g/L. (b) Histogram of the Ra/Ba ToF-SIMS intensity ratio
262 obtained from 400 integrated measurement points of AL 0.5 g/L.

263 The distribution of Ra/Ba intensity ratios in the SL sample is narrow and ends at about 1 x 10^{-2}
264 whereas the distribution in the AL sample is broader and exhibits a small number of individual
265 grains which contain much more Ra than the average ratio predicted from macroscopic
266 experiments (Figure 3 b). No systematic trend with respect to the grain size could be observed
267 for the SL Ra/Ba intensity ratios. This may be taken as an indirect proof that Ra is not enriched
268 at the mineral surfaces but distributed into the barite crystals during recrystallization. As a result

269 of the ToF-SIMS investigations, it is now possible to distinguish between the two possible
270 scenarios of Ra uptake by already existent barite, (1) formation of a $Ba_{1-x}Ra_xSO_4$ solid solution
271 surface layer on barite or (2) a complete recrystallization, leading to homogenous
272 $Ba_{1-x}Ra_xSO_4$ crystals. A complete recrystallization of barite into a $Ba_{1-x}Ra_xSO_4$ solid solution can
273 be proposed. Therefore, the treatment of the $Ba_{1-x}Ra_xSO_4$ solid solution with thermodynamic
274 tools as shown e.g. in Vinograd et al., 2014 (17) can now be justified. As a consequence,
275 geochemical modeling applied for the safety assessment of deep geological disposal of nuclear
276 waste and environmental issues related to TENORM can now include this solid solution system.
277
278 **Effect of Ra on barite recrystallization**
279 **Evolution of morphology and grain size distribution**
280 The combination of the ToF-SIMS analyses and the observed Ra uptake from the solution
281 show that Ra is efficiently taken up by pure barite. A detailed SEM investigation was performed
282 to identify the influence of the presence of Ra on the recrystallization of barite. Particle size
283 distributions (PSD) were determined to quantify the observations by SEM with more extended
284 statistical information about the barite particles, similar to earlier studies e.g. Simonsen et al.
285 2011 (23).
286 Two reference samples, one SL (Figure 4 a) and one AL barite (Figure 5 a), were aged in
287 parallel experiments with a solid to liquid ratio of 5 g/L under the same conditions as the ^{226}Ra
288 uptake experiments. SEM observation of the SL sample before (Figure 4 a) and after (Figure 4 b)
289 the experiments indicates that there is no significant change of the morphology after 443 days.
290 At the beginning of the experiments, the SL barite sample was characterized by a narrow grain
291 size distribution with grain sizes between ~ 6 and 45 µm (see Table S1 and Figure S1, supporting

information). The changes in the PSD of the reference without Ra due to aging are within the error of the analysis.

After being in contact for 443 days with a Ra spiked solution, the morphology of SL crystals changed only slightly. However, in contrast to the reference, the grains of this sample were observed to be grown together with a defined orientation, forming large aggregates (Figure 4 c,d). Even in the presence of Ra, the narrow grain size distribution remains mainly unchanged with only insignificant differences between minimum and maximum values of the PSD (Supporting information Table S1). The apparent changes in the mass based grain size distribution are due to individual large grains which have a high impact here but not in the frequency based PSDs of SL after aging with and without Ra.

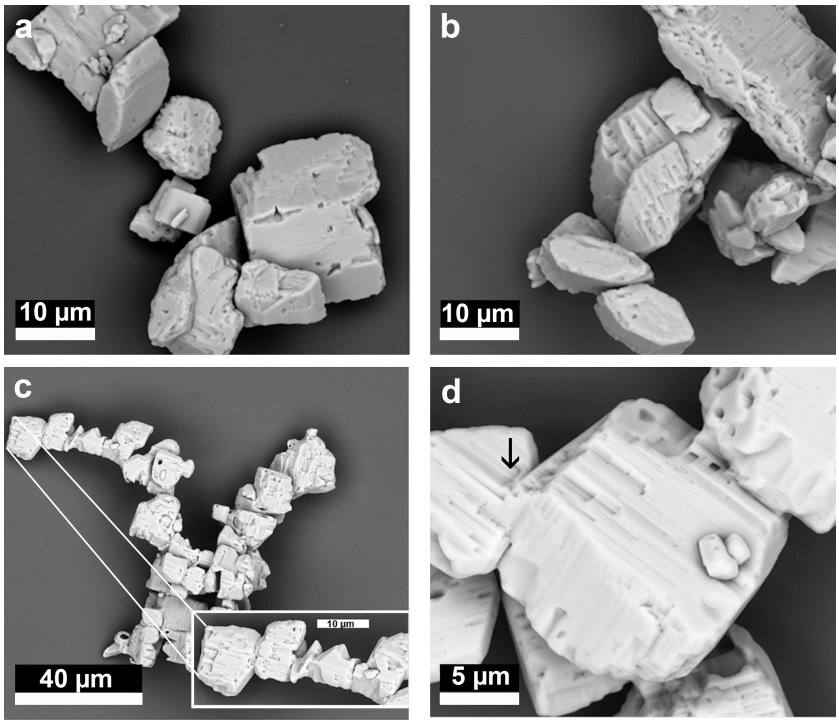

Figure 4. (a) Morphology of individual grains of reference SL without Ra at the beginning of the experiment and (b) at the end of the reference experiment after 443 days; (c) Morphology of SL barite 5 g/L after 443 days in contact with the Ra solution. Grains are grown together and form

large aggregates. (d) Detail of an aggregate. The arrow marks the area, where two grains are grown together in an oriented way.

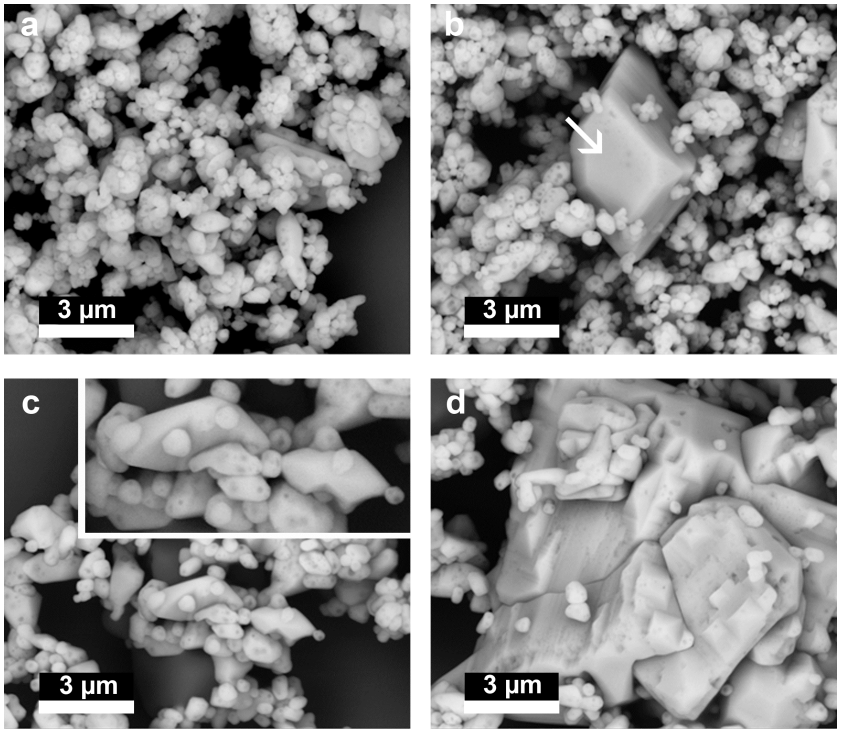

Figure 5. (a) Morphology of reference AL without Ra at the beginning of the experiment and (b) at the end of the reference experiment after 443 days. A newly formed large particle is marked with an arrow; (c) Morphology of AL after 443 days in contact with the Ra solution for experiments with 0.5 g/L barite. The zoomed inset illustrates details of the particle shape (d). Large grains > 10 µm are grown, assimilating smaller grains.

At the beginning of the experiments, the AL barite sample was characterized by a wide grain size distribution with grain sizes between ~ 0.2 and 2.2 µm (see Table S1, supporting information). Already without Ra, newly formed, larger idiomorphous crystals with a typical grain size larger than 3 µm appear in the reference AL sample after 443 days (Figure 5 b, large particle marked with an arrow). In comparison, the original small grains are typically smaller

319 than 1 µm (Figure 5 a). After 443 days, the morphology and shape of the small grains didn't
320 change significantly within this reference sample (Figure 5 b).

321 In comparison with the reference experiment, an additional change of the AL particle
322 morphology in the presence of Ra was observed after 443 days. The small particles were less
323 rounded and elongated with sharp edges, and less pores on the surface (Figure 5 c, zoomed
324 inset). The grain size of the small particles increased visibly. Furthermore, small grains were
325 assimilated by the growth of large idiomorphous crystals which are up to > 10 µm in size (Figure
326 5 d).

327 For the AL sample, the quantification was carried out for the fine particles only as the large
328 particles > 5 µm were statistically not relevant. The initial AL type barite is characterized by a
329 wide PSD, covering more than one order of magnitude in the mass based representation (Figure
330 6).

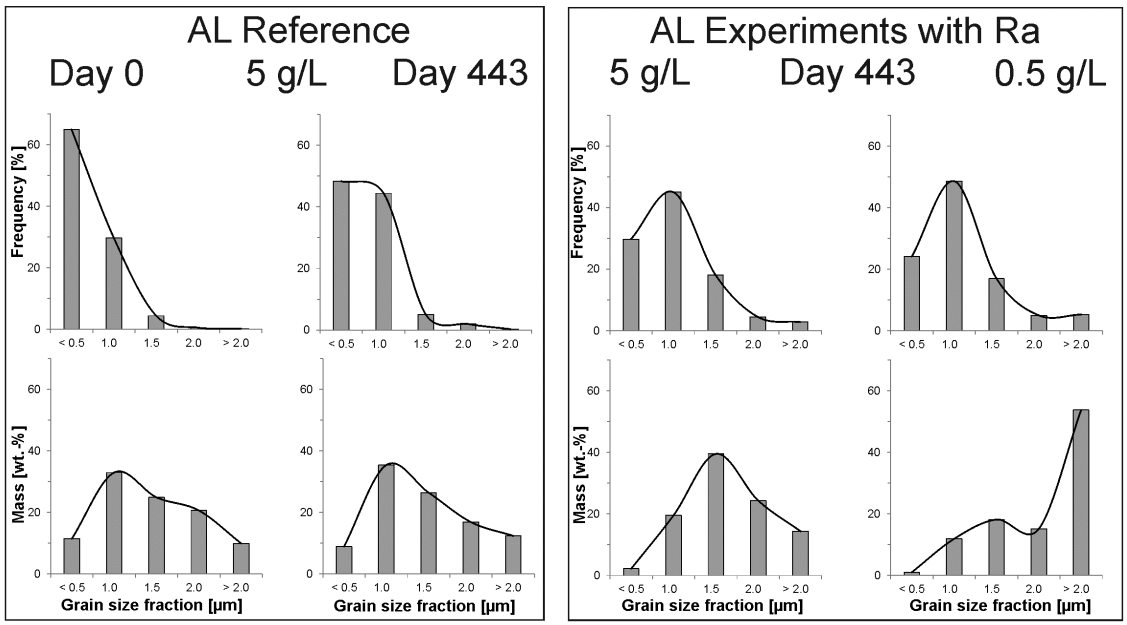

331

332 **Figure 6.** PSD based on frequency (upper histograms) and calculated equivalent mass (lower
333 histograms) of AL barite. Left: Reference experiments without Ra; right: Experiments with Ra.

334 A slight shift of the PSD towards higher grain sizes was observed on the AL reference sample
335 which was aged for 443 days. This is more clearly detected in the frequency based PSD. Mainly,
336 the very small grains in the fraction < 0.5 µm were shifted to the fraction 0.5 – 1.0 µm. In the
337 presence of Ra, not only new large grains (> 2 µm) appeared as described above but also a
338 significant coarsening of the small grains can be deduced from the PSD (Figure 6, supporting
339 information Table S1). The most significant effect is visible in the mass based PSD of the
340 0.5 g/L AL sample.
341 In summary, the presence of Ra was found to affect the recrystallization process, however in a
342 different way for the two studied barites. The wide PSD of AL barite is changed during the
343 recrystallization of barite in the presence of Ra compared to a Ra free reference. The mechanism
344 of Ostwald ripening is related to the coarsening of some particles while very small particles
345 dissolve. Ostwald ripening is a grain size coarsening due to the minimization of the interfacial
346 energy (24). The existence of even larger newly formed crystals in the experiment with Ra
347 indicates an additional effect of the solid - aqueous disequilibrium, in addition to the surface
348 energy minimization.
349 On the other hand, the particle size of the SL sample remains more or less constant. Here, a
350 distinctively different mechanism of coarsening appears to occur i.e. the formation of orientated
351 aggregates. This effect has been described in the literature to occur preceding Ostwald ripening,
352 eventually also resulting in the occurrence of large particles. Such effects were observed by Jia &
353 Goa, 2008 (25), who investigated the growth of well-defined cubic hematite single crystals due
354 to the oriented aggregation of particles and Ostwald ripening. There, particles formed
355 agglomerates which eventually made up single crystals.
356

Environmental Implications

Recrystallization of barite and simultaneous uptake of Ra has been proven to be a relevant mechanism for the retention of Ra in the environment. Considering the relevant time scales of nuclear waste disposal (up to several 100,000 years) this process is comparatively fast. However, compared to co-precipitation as the proposed main mechanism of Ra-removal related to TENORM, recrystallization it is a rather slow process. Thus, the amount of Ra taken up by barite on the scale of days during recrystallization is not representative for the long-term. In the long term, the Ra concentration in an aqueous solution in contact with pre-existing barite will significantly decrease due to the thermodynamics of $(Ba,Ra)SO_4$ solid solutions. However, the effect of other ions such as Sr or Pb which are also known to form solid solutions with barite will need to be studied to extend the system $(Ba,Ra)SO_4$ investigated here to a broader range of environmental conditions.

Acknowledgements

The authors would like to thank three anonymous reviewers and the editor for improving the manuscript. The research leading to these results has received partial funding from the European Atomic Energy Community's Seventh Framework Programme (FP7/2007-2011) under grant agreement n° 269688. We are grateful to Fabian Sadowski, Juliane Weber, Guido Deissmann and Giuseppe Modolo for their support.

Supporting Information Available

Supporting information includes details on the particle size distributions discussed above. This information is available free of charge via the Internet at http://pubs.acs.org/ .

TOC Art

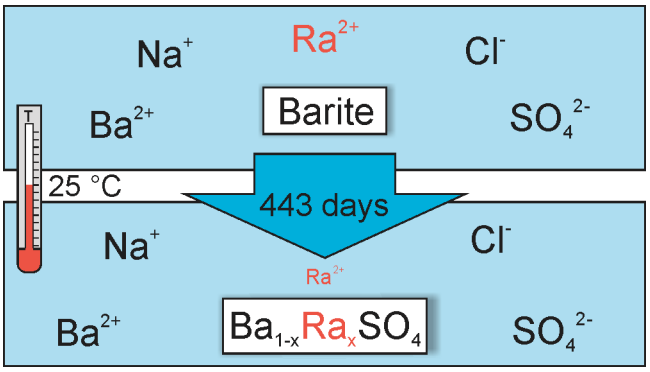

AUTHOR INFORMATION

Corresponding Author

* Phone: ++49 2461 612752; fax: ++49 2461 612450; e-mail: m.klinkenberg@fz-juelich.de

References

(1) Doerner, H. A.; Hoskins, W. M., Co-precipitation of radium and barium sulfates. *Journal of the American Chemical Society* **1925,** *47*, 662-675.

(2) Carvalho, F. P.; Oliveira, J. M.; Neves, M. O.; Abreu, M. M.; Vicente, E. M., Soil to plant (Solanum tuberosum L.) radionuclide transfer in the vicinity of an old uranium mine. *Geochemistry: Exploration, Environment, Analysis* **2009,** *9* (3), 275-278.

(3) Rutherford, P. M.; Dudas, M. J.; Arocena, J. M., Heterogeneous distribution of radionuclides, barium and strontium in phosphogypsum by-product. *Science of The Total Environment* **1996,** *180* (3), 201-209.

(4) Burnett, W. C.; Elzerman, A. W., Nuclide migration and the environmental radiochemistry of Florida phosphogypsum. *Journal of Environmental Radioactivity* **2001,** *54* (1), 27-51.

(5) Fisher, R. S., 1998. Geologic and Geochemical Controls on Naturally Occurring Radioactive Materials (NORM) in Produced Water from Oil, Gas, and Geothermal Operations. *Environmental Geosciences* **5**, 139-150.

(6) Martin, A. J.; Crusius, J.; McNee, J. J.; and Yanful, E. K., 2003. The mobility of radium-226 and trace metals in pre-oxidized subaqueous uranium mill tailings. *Appl Geochem* **18**, 1095-1110.

(7) Liu, D. J.; Hendry, M. J., Controls on (226)Ra during raffinate neutralization at the Key Lake uranium mill, Saskatchewan, Canada. *Applied Geochemistry* **2011,** *26* (12), 2113-2120.

(8) Zhang T., Gregory K., Hammack R. W. and Vidic R. D., Co-precipitation of Radium with Barium and Strontium Sulfate and its Impact on the Fate of Radium during Treatment of Produced Water from Unconventional Gas. *Environ. Sci. Technol.* **2014**, *48*, 4596–4603.

(9) Norrby, S.; Andersson, J.; Dverstorp, B.; Kautsky, F.; Lilja, C.; Sjöblom, R.; Sundström, B.; Toverud, Ö.; Wingefors, S. *SKI SITE-94 Saekerhetsanalys foer Djupfoervar iett Kristallint berg*; Statens Kaernkraftsinspektion: 1997.

(10) Grandia, F.; Merino, J.; Bruno, J., Assessment of the radium-barium co-precipitation and its potential influence on the solubility of Ra in the near-field, SKB Technical Report TR-08-07. 2008.

(11) Berner, U.; Curti, E., 2002. Radium solubilities from SF/HLW wastes using solid solution and co-precipitation models. Internal Report TM-44-02-04, Paul Scherer Institut, Villigen, Switzerland.

(12) Kulik, D., Berner, U., and Curti, E., 2004. Modelling chemical equilibrium partitioning with the GEMS-PSI code. PSI Scientific Report 2003. Paul Scherrer Institute, Villigen, Switzerland.

(13) Bruno, J., Bosbach, D., Kulik, D., and Navrotsky, A., 2007. Chemical thermodynamics of solid solutions of interest in radioactive waste management: A state-of-the art report In: Mompean, F. J., Illemassene, M., and Perrone, J. Eds.) Chemical Thermodynamics Series 10. OECD-Nuclear Energy and Safety, Paris.

(14) Rosenberg, Y. O.; Metz, V.; Ganor, J., Co-precipitation of radium in high ionic strength systems: 1. Thermodynamic properties of the Na-Ra-Cl-SO(4)-H(2)O system - Estimating Pitzer parameters for RaCl(2). *Geochimica et Cosmochimica Acta* **2011,** *75* (19), 5389-5402.

(15) Rosenberg, Y. O.; Metz, V.; Oren, Y.; Volkman, Y.; Ganor, J., Co-precipitation of radium in high ionic strength systems: 2. Kinetic and ionic strength effects. *Geochimica et Cosmochimica Acta* **2011,** *75* (19), 5403-5422.

(16) Rosenberg, Y.O., Sadeh, Y., Metz, V., Pina, C.M., Ganor, J., Nucleation and growth kinetics of $Ra_xBa_{1-x}SO_4$ solid solution in NaCl aqueous solutions, *Geochimica et Cosmochimica Acta* **2013**, doi: http://dx.doi.org/10.1016/j.gca.2013.09.041

(17) Vinograd, V. L.; Brandt, F.; Rozov, K.; Klinkenberg, M.; Refson, K.; Winkler, B.; Bosbach, D., Solid-aqueous equilibrium in the BaSO4-RaSO4-H2O system: first-principles

437 calculations and a thermodynamic assessment. *Geochimica et Cosmochimica Acta* 122 (**2013**)
438 398–417

439 (18) Curti, E.; Fujiwara, K.; Iijima, K.; Tits, J.; Cuesta, C.; Kitamura, A.; Glaus, M. a.; Müller,
440 W., Radium uptake during barite recrystallization at 23±2°C as a function of solution
441 composition: An experimental 133Ba and 226Ra tracer study. *Geochimica et Cosmochimica*
442 *Acta* **2010,** *74* (12), 3553-3570.

443 (19) Bosbach, D.; Böttle, M.; Metz, V., Experimental study on Ra2+ uptake by barite
444 (BaSO4), SKB Technical Report TR-10-43. 2010.

445 (20) Ekberg C, 1999. Uncertainties in actinide solubility calculations illustrated using the Th-
446 OH-PO4system. Ph. D. thesis, Chalmers University of Technology, Göteborg, Sweden.

447 (21) J.C. Vickerman and D. Briggs (Ed), ToF:SIMS Surface Analysis by Mass Spectrometry,
448 *IM Publications and Surface Spectra Limited* (2001)

449 (22) Grehl, T.; Möllers, R.; Niehuis, E.; Low energy dual beam depth profiling: influence of
450 sputter and analysis beam parameters on profile performance using TOF-SIMS, *Applied Surface*
451 *Science* 203-204 (**2003**) 277-280

452 (23) Simonsen, S.B.; Chorkendorff, I.; Dahl, S.; Skoglundh, M.; Sehested, J.; Helveg, S.,
453 Ostwald ripening in a Pt/SiO2 model catalyst studied by in situ TEM, *Journal of Catalysis* 281
454 (**2011**), 147-155.

455 (24) Ostwald, W. (1896): Lehrbuch der Allgemeinen Chemie, Vol. 2, part 1, Leipzig, Germany

456 (25) Jia, B.; Gao, L., Growth of Well-Defined Cubic Hematite Single Crystals: Oriented
457 Aggregation and Ostwald Ripening. *Crystal Growth & Design* **2008,** *8* (4), 1372-1376.